Effect of Antenna Ports on TOA Estimation with 4G LTE Signals in Urban Mobile Environments

Chun Yang Thomas Pany Petra Weitkemper
QuNav *Universität der Bundeswehr München*

BIOGRAPHIES

Dr. Chun Yang received his title of Docteur en Science from the Université Paris-Saclay (previously known as the Université de Paris-Sud, Paris XI). After postdoctoral research at the University of Connecticut (Storrs, CT), he has been working on adaptive array, synthetic aperture, and baseband signal processing for GNSS, radar, and communications signals and systems; nonlinear state estimation in target tracking, integrated inertial and distributed collaborative navigation; and optimization in resource management and information fusion. Dr. Yang received the ION Samuel M. Burka Award in 2007.

Dr. Thomas Pany is with the Universität der Bundeswehr München where he leads the satellite navigation unit LRT 9.2 of the Institute of Space Technology and Space Applications (ISTA). He teaches navigation focusing on GNSS, sensors fusion and aerospace applications. Within LRT 9.2 a good dozen of full-time researchers investigate GNSS signal design, GNSS transceivers and high-integrity multi-sensor navigation (inertial, LiDAR) and are also developing a modular UAV-based GNSS test bed. ISTA also develops the MuSNAT GNSS software receiver and recently focuses on Smartphone positioning and GNSS/5G integration. He has a PhD from the Graz University of Technology and worked in the GNSS industry for seven years.

Dr. Petra Weitkemper received her Dr.-Ing. Degree from University of Bremen, Germany. After several years as Senior Researcher in the Wireless Research Group at DOCOMO Eurolabs she became professor for communication systems at the Bundeswehr University in Munich. Her research focus is on the physical layer of mobile communication systems and she has been working on waveform design, multiple access schemes, signal processing and channel coding in LTE and 5G, respectively, including participation in 3GPP RAN1 meetings and contribution to EU-funded projects ARTIST4G, METIS and METIS II.

ABSTRACT

The fourth generation (4G) long term evolution (LTE) standard signals are well specified in the 3GPP standards. However, some aspects are left to operators as implementation options that depend on the actual deployment environment and local traffic patterns. To better understand such practical issues of in-the-air LTE signals, several experiments were carried out near Munich, Germany, which collected data of frequency division duplex (FDD) downlink frames for the analysis presented in this paper.

From experimental data, LTE signals are observed in multiple frequency bands at a site and signals from different cells may be present on the same frequency carrier. In the latter case, signaling patterns are found to be coordinated in the data in such a way to avoid collision among the neighboring cells. Various orthogonal frequency division multiplexing (OFDM) signal components, namely, cyclic prefix (CP), primary synchronization signal (PSS), secondary synchronization signal (SSS), and cell-specific reference signals (CRS) are described in the paper together with their properties, rationale of design, and possible ways to exploit them for navigation, that is, generation of the time of arrival (TOA) estimates and pseudoranges for positioning.

As a focus of this paper, antenna port (AP) is a unique concept introduced in 4G LTE and its actual implementation depends on a particular operator. AP is a logical entity and cannot be simply equated to a physical antenna. It is important as it is one of the key parameters that define the CRS. In other words, each antenna port is associated with a specific reference signal; and a receiver needs to use this reference signal to estimate the channel corresponding to the specific antenna port regardless of its physical origin. As such, the use of antenna ports does not cause any problem in channel estimation/equalization and subsequent data demodulation/decoding for communications. However, when CRS is used to estimate TOA from the channel impulse response (CIR) for timing, ranging, and ultimately positioning, it may present a potential ambiguity as to where the physical transmit antenna's phase center is for the purpose of precise ranging. Unfortunately, this critical aspect is not well addressed in the 4G LTE-based opportunistic positioning literature. In this paper, experimental data are used to illustrate the effect of antenna ports on TOA estimation. Understanding of such effects is prerequisite for precision timing and ranging especially with carrier phase. The paper provides essential and insightful information directly useable for developing advanced TOA estimation algorithms and ultimately for navigation with LTE signals.

 https://doi.org/10.33012/2020.17524

INTRODUCTION

The orthogonal frequency-division multiplexing (OFDM) modulation is adopted by many modern wireless communication systems (4G LTE [1] and WiMAX [2]), wireless local area network (Wi-Fi [2], DSRC [3]), and digital television (DVB-T [4], ISDB-T [5], DTMB [6], ATSC 3.0 [7]) as well as ultra-wideband radar [8]. OFDM signals have been studied as one type of signals of opportunity for positioning, navigation, and timing (PNT) in Global Navigation Satellite System (GNSS)-challenged environments [9 – 27].

OFDM offers high spectral efficiency thanks to the use of orthogonal subcarriers, which overlap but do not interfere, with the properly chosen subcarrier spacing and pulse shaping. With its bandwidth being small as compared to the coherent bandwidth of the channel, each subcarrier is only distorted by flat-fading, which can be easily corrected using simple channel estimation and equalization techniques (i.e., one parameter per subcarrier). More importantly, a guard interval is inserted between successive OFDM symbols to avoid inter-symbol interference (ISI), that is, there is no ISI if the maximum delayed echo of the preceding symbol (due to multipath and channel spread) does not exceed the guard interval into the subsequent symbol. In 4G LTE and many other systems, an exact copy of the end of an OFDM symbol waveform, called cyclic prefix (CP), is transmitted in the guard interval ahead of the whole symbol. The insertion of CP makes the waveform periodic, thus tolerating small timing errors and simplifying the equalization. That is, only a phase distortion is introduced to the useful symbol if the processing at reception starts earlier into the CP. Furthermore, a multipath signal with a delay smaller than the CP duration is merely an additive circularly shifted version of the original signal, which affects the symbol by a complex multiplicative distortion and can be corrected by the channel equalization.

With CP, OFDM has a built-in tolerance to a small sync error and the robustness against multipath on the order of a CP duration. However, the OFDM modulation suffers from high peak to average power ratio (PAPR), which demands high dynamic range, especially in the power amplifier (PA) of transmitters. Otherwise, the PA would enter the nonlinear region of saturation when amplifying signals of large amplitude. In addition, guard bands are required to reduce possible inter-band interference (IBI) so that the signal remains within its band in the presence of clock drift and Doppler frequency shift. The inter-carrier (subcarrier) interference (ICI) can be avoided if the orthogonality of subcarriers is maintained, which places high demands on processing of OFDM baseband signals in the receiver to deal with such issues as carrier frequency offset (CFO), carrier phase offset (CPO), sampling clock offset (SCO), symbol timing offset (STO), IQ imbalance and DC offset, and power amplifier nonlinearity (constellation distortion and inter-modulation distortion) [28, 29].

By design, the 4G LTE signals contain a number of cyclic patterns that repeat in time and frequency to facilitate timing synchronization, frequency error estimation, and channel estimation. For communications, these signal components are considered "overhead," serving the purpose of extracting information-carrying symbols for decoding. From the point of view of demodulating an OFDM symbol for communications, only a coarse synchronization is required thanks to the CP as explained above.

However, for the purpose of ranging and positioning, more accurate techniques are required for timing, which can locate in time the true starting point of each OFDM symbol, i.e., its time of arrival (TOA) in the receiver's time. In addition to cyclic prefixes, reference symbols and other synchronization signals embedded in OFDM signals have been used for fine TOA estimation [9 – 27]. When used as signals of opportunity for navigation, they provide TOA estimates, and changes in these variables can be related to the receiver displacement. Indeed, successful use of LTE signals has been reported in the literature for ground vehicles, airborne platforms, and indoor positioning.

Even though LTE signals are well specified in the 3GPP standards, some aspects are not mandatory but optional and therefore left to operators as implementation options that depend on the actual deployment environment and local traffic conditions. To better understand the practical aspects of in-the-air LTE signals, several experiments were carried out near Munich, Germany and the data collected were analyzed for TOA estimation as presented in this paper.

From experimental data, LTE signals are observed in multiple frequency bands at a site and signals from different cells may be present on the same frequency carrier. In the latter case, signaling patterns are found to be coordinated in the data in such a way to avoid collision among the neighboring cells. Various OFDM signal components, namely, cyclic prefix (CP), primary synchronization signal (PSS), secondary synchronization signal (SSS), and cell-specific reference signals (CRS) are available for the purpose of navigation, that is, generation of the time of arrival (TOA) estimates and pseudoranges for positioning.

The focus of this paper is on antenna port (AP), which is a unique concept introduced in 4G LTE. However, its actual implementation depends on a particular operator. AP is a logical entity and cannot be simply equated to a physical antenna. It is important as it is one of the key parameters that define the CRS. In other words, each antenna port is associated with a specific reference signal; and a receiver needs to use this reference signal to estimate the channel corresponding to the specific antenna port regardless of its physical origin. As such, the use of antenna ports does not cause any problem in channel estimation/

equalization and subsequent data demodulation/decoding for communications. However, when CRS is used to estimate TOA of the channel impulse response (CIR) for timing, ranging, and ultimately positioning, it may present a potential ambiguity as to where the physical transmit antenna's phase center is. Unfortunately, this critical aspect is not well addressed in the 4G LTE-based opportunistic positioning literature. In this paper, experimental data are used to illustrate the effect of antenna ports on TOA estimation. Understanding of such effects is prerequisite for precision timing and ranging especially with carrier phase.

The rest of the paper is organized as follows. Sample waveforms and inner structures of 4G LTE signals are first presented using collected experimental data. The LTE frequency division duplex (FDD) downlink frame is then described in terms of the time-frequency diagram together with synchronization and reference signals. Antenna ports are introduced next with their use in generating CRS sequences. Effects of APs on TOA estimates and pseudoranges are illustrated with experimental data before presenting the conclusions.

EXPERIMENTAL DATA COLLECTION AND 4G LTE WAVEFORMS

The experimental data were collected in the vicinity of the campus of the Bundeswehr University near Munich, Germany, as shown in Fig. 1. In this area, three network operators are active rendering the base station setup quite complex. It was found that reception of a sufficient number of LTE signals (to be able to compute a position fix) requires careful selection of two frequency bands. Static and dynamic tests were conducted. A dynamic trajectory on the Google map is shown in Fig. 1 together with the photos of the two visually verified cell towers on rooftop. However, the positions of cell towers reported in open databases were found to be not up to date and/or partly incorrect.

Fig. 1 – Test Environment, Test Trajectory, and Cell Tower Sites

In the data collection setup, a National Instruments USRP frontend with two RF inputs was used together with a passive LTE antenna and an in-house data logging software. We selected two of the three frequency bands in 800 MHz, 1.8 GHz, and 2.1 GHz at a time and applied complex I/Q sampling at the rate of 20 MHz. Fig. 2(a) is a snapshot of the real part of a complex baseband waveform of a LTE signal resampled to 15.36 MHz, which has significant variations in its amplitude (42 spikes over 21 slots). Fig. 2(b) shows the spectrum of a signal at 796 MHz, whose bandwidth is 5 MHz with an adjacent signal visible. Fig. 2(c) shows the spectrum of another signal at 2135.2 MHz, whose bandwidth seems larger than 5 MHz but narrower than 10 MHz.

Fig. 2(d) shows another example of the real part of a complex baseband waveform resampled at 1.92 MHz where periodic gaps are visible, which correspond to transitions between subframes (two slots over 1 ms), the schedulable units for continuous transmission. Note that the purple * and yellow o mark the start of PSS and SSS symbols, respectively, while the red x indicates the start of seven OFDM symbols in a slot. The particular slot shown in Fig. 2(e) happens to be an empty slot where the 1st and 4th OFDM symbols are populated with reference signals. Fig. 2(f) shows the detail of an OFDM symbol where the cyclic prefix of 9 samples are highlighted with a purple line segment as compared to the original signal at the end of this OFDM symbol highlighted with a green line segment. There are six periods visible in this waveform.

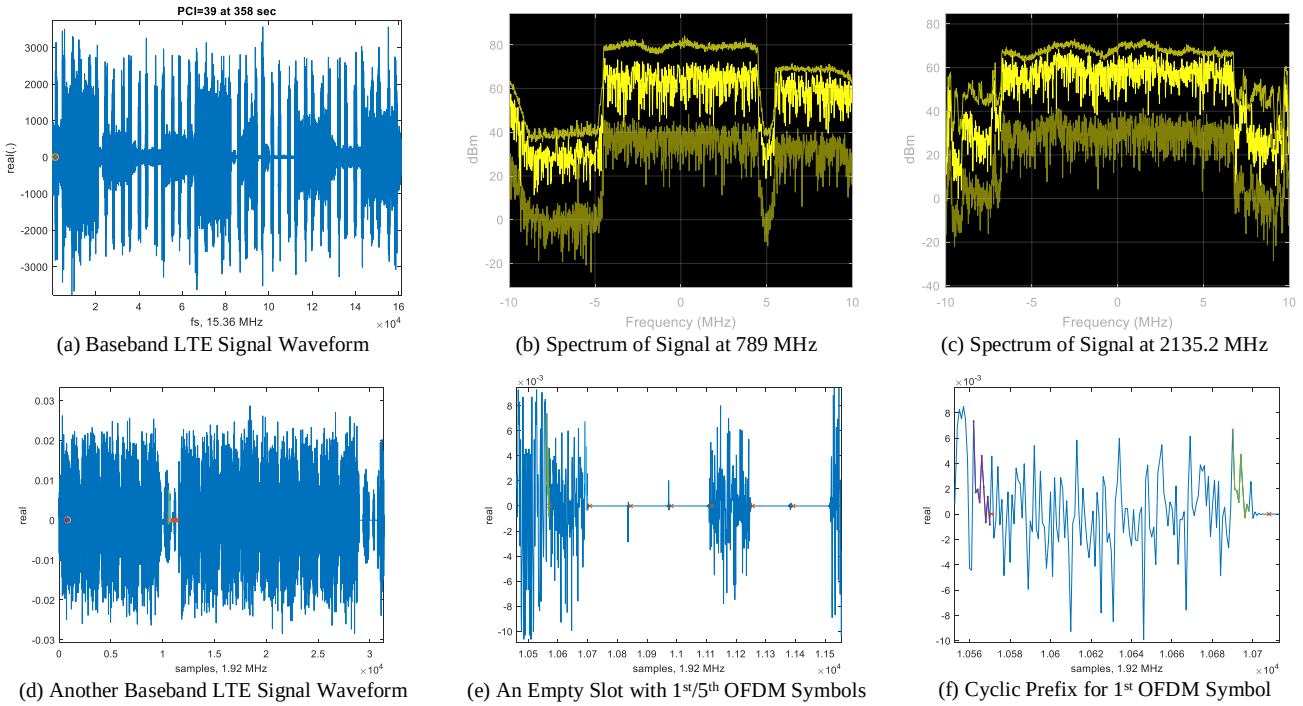

(a) Baseband LTE Signal Waveform (b) Spectrum of Signal at 789 MHz (c) Spectrum of Signal at 2135.2 MHz

(d) Another Baseband LTE Signal Waveform (e) An Empty Slot with 1st/5th OFDM Symbols (f) Cyclic Prefix for 1st OFDM Symbol

Fig. 2 – Sample LTE Signal Waveform and Spectra

LTE FDD DOWNLINK FRAME AND REFERENCE SIGNALS

In this paper, we consider the downlink frame of a LTE FDD signal illustrated in Fig. 3 as a time-frequency (resource) diagram. Along the time axis, each radio frame is 10 ms long, divided into ten subframes of 1 ms each. Each subframe has two slots of 0.5 ms each, and each slot comprises seven OFDM symbols with normal CP (or six OFDM symbols with extended CP). The useful part of OFDM symbols is the same in all symbols, equal to 66.67 μs (corresponding to 15 kHz subcarrier spacing), but the CP for the first OFDM symbol in a slot (5.1 μs) is slightly longer than that of the other six OFDM symbols (4.7 μs). Along the frequency axis, the downlink may operate in one of six transmission bandwidths from 1.4 MHz up to 20 MHz as listed in Table 1. The band is divided to subcarriers with 15 kHz spacing. The occupied subcarriers in the band center constitute the effective bandwidth with guard subcarriers on both ends of the band.

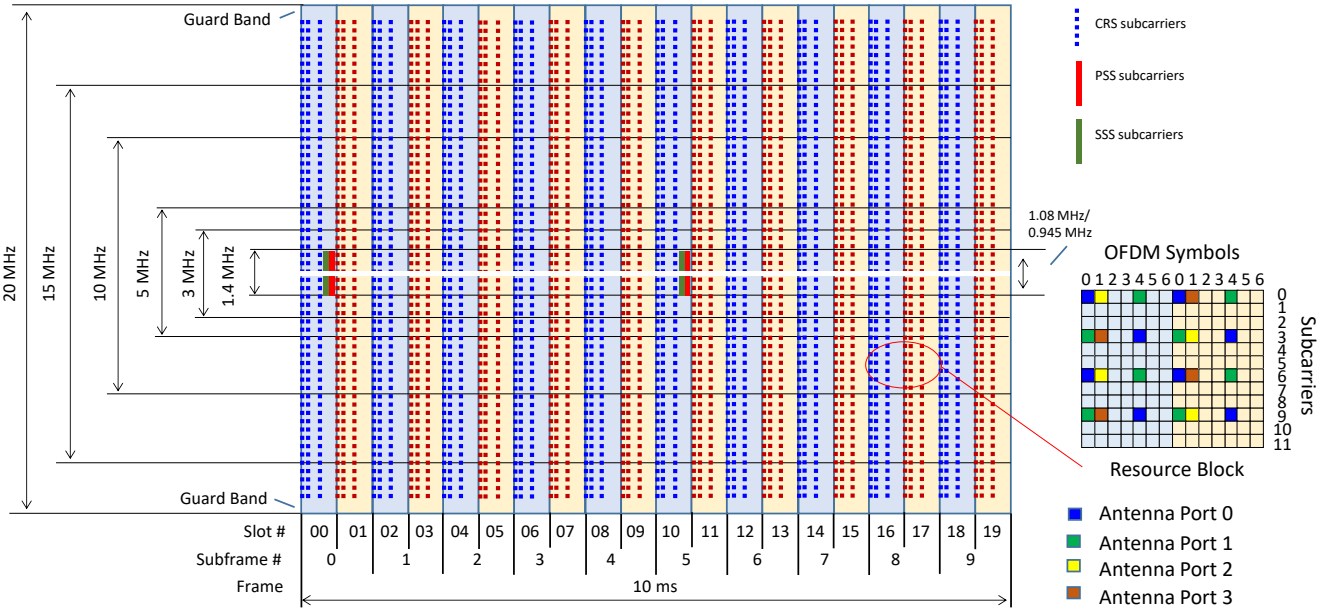

Fig. 3 – Timing Signals in Time-Frequency (Resource) Diagram of a LTE Downlink Frame

Table 1 – Key Parameters of LTE Downlink OFDM Symbols

Channel Bandwidth (MHz)	1.4	3	5	10	15	20
Frame / Subframe Duration (ms)	10 / 1					
Subcarrier Spacing (kHz)	15					
Useful Time for FFT (μs)	66.67					
FFT Size (Total Subcarriers)	128	256	512	1024	1536	2048
Occupied Subcarriers (Including DC)	73	181	301	601	901	1201
Guard Subcarriers	55	75	211	423	635	847
CP: 1st/2nd-7th Symbol (Samples)	10 / 9	20 / 18	40 / 36	80 / 72	120 / 108	160 / 144
Total Samples: 1st/2nd-7th Symbol (Samples)	138 / 137	276 / 274	552 / 548	1104 / 1096	1656 / 164	2208 / 2192
Effective Bandwidth (MHz)	1.08	2.7	4.5	9	13.5	18
Resource Blocks	6	15	25	50	75	100
Bandwidth Efficiency	77.1%	90%	90%	90%	90%	90%
Sampling Rate (MHz)	1.92	3.84	7.68	15.36	23.04	30.72

In the time-frequency diagram, a subcarrier and an OFDM symbol is called a resource element (RE), and twelve subcarriers and a subframe (two slots) constitute a resource block (RB). RB is the scheduling unit of transmission.

Note that location of the secondary synchronization signal (SSS) with respect to the primary synchronization signal (PSS) reveals the transmission mode. It is FDD if SSS is one OFDM symbol earlier than PSS; and time division duplex (TDD) if three OFDM symbols earlier. Similarly, the OFDM symbol type can be determined to be either a normal CP (7 OFDM symbols per slot) or an extended CP (six OFDM symbols per slot). In this paper, we focus on FDD OFDM symbols with normal CP.

Primary Synchronization Signal (PSS)

As shown in Fig. 3, timing of a radio frame is indicated by the primary synchronization signal (PSS), which is transmitted as the last symbol of the first slot in the first and sixth subframes (1st and 11th slots), i.e., every 5 ms. PSS is specified as one of three orthogonal length-62 Zadoff-Chu sequences [30, 31], mapped onto 62 subcarriers located symmetrically around the DC-subcarrier (over a bandwidth of 0.945 MHz). Each PSS sequence corresponds to a sector identity within a group of three sectors ($N_{Id}^{(2)}$ = 0, 1, 2). As a result, detection of a PSS provides (i) symbol boundary, (ii) slot boundary, (iii) frame sync to 5 ms, and (iv) sector ID $N_{Id}^{(2)}$.

Secondary Synchronization Signal (SSS)

Ahead of PSS in a FDD frame is the secondary synchronization signal (SSS), which is also specified in the frequency domain as one of one-thousand-and-eight (1008) length-62 sequences, mapped onto 62 subcarriers located symmetrically around the DC-subcarrier (also over a bandwidth of 0.945 MHz). A SSS sequence is an interleaved concatenation of two length-31 binary sequences, which are cyclic-shifted and scrambled differently depending on the group identity ($N_{Id}^{(1)}$ = 0, 1, …, 167), sector identity ($N_{Id}^{(2)}$ = 0, 1, 2), and subframe number (subframe = 0, 5). First detection of PSS can reduce the number of possibilities for SSS to 168 for either subframe 0 or subframe 5, respectively, because the sector identity is already known form the PSS. Detection of a SSS thus provides (i) symbol boundary, (ii) frame sync (subframe 0 or subframe 5), (iii) frame structure (FDD or TDD), (iv) group ID $N_{Id}^{(1)}$, and (v) a rough estimate of the fractional frequency offset (FFO) as compared to the subcarrier grid from the pair of SSS and PSS.

Physical Cell Identity (PCI)

The physical cell identity (PCI) (N_{Id}^{Cell} = 0 to 503) can be determined from the group ID $N_{Id}^{(1)}$ and sector ID $N_{Id}^{(2)}$ as

$$N_{Id}^{Cell} = 3N_{Id}^{(1)} + N_{Id}^{(2)} \quad (1)$$

Roughly speaking, the group ID, $N_{Id}^{(1)}$, points to a cell tower, the sector ID, $N_{Id}^{(2)}$, points to an antenna array on the tower, and the cell ID (PCI), N_{Id}^{Cell}, refers to the RF footprint from the antenna array on the tower, which covers a user equipment (UE) on the ground. Typically, each cell tower can have up to three antenna arrays mounted on a triangular structure, each covering a 120° sector around the tower. In LTE, what is equivalent to a base transceiver station (BTS) in GSM is the so-called Evolved NodeB (eNodeB or eNB). Note that in LTE eNB is a logical node. A common implementation of an eNodeB is a three-sector site with a baseband processing unit handling calls in the three cells. But a large number of indoor cells or cells along a highway may be connected to a single eNodeB.

Other Downlink Data

Not shown in Fig. 3 are the resources (OFDM symbols and subcarriers) designated for the physical broadcast channel (PBCH) located at the second timeslot (first 4 OFDM symbols) on the first subframe (within the 1.08 MHz bandwidth), from which the master information block (MIB) can be decoded. MIB contains information about system bandwidth and system frame number among others. At least four frames are required to retrieve the information. The downlink control channels (PDCCH) are located at the beginning of every subframe (first three OFDM symbols). The first system information block (SIB1), also part of the

PBCH, contains cell ID, public land mobile network (PLMN) identity, and scheduling of transmission of other system information among others. Since we are interested in cyclic patterns and reference signals for timing, the aspect of data demodulation is not considered in this paper. Note that, however, decision-directed data-feedback can be used for refined synchronization [32].

ANTENNA PORT (AP), CELL-SPECIFIC REFERENCE SIGNAL (CRS), AND CHANNEL IMPULSE RESPONSE (CIR)

Starting LTE Release 10, there are 22 antenna ports (APs) defined for different multi-antenna transmission purposes and much more in 5G NR [47] as illustrated in Fig. 4. Antenna ports 0, 1, 2, 3 are considered to be "CRS antenna ports," which are used primarily to estimate the channel transfer function (CTF) in the frequency domain for OFDM subcarrier equalization and demodulation, and its time-domain counterpart, the channel impulse response (CIR), can serve our purpose of TOA estimation.

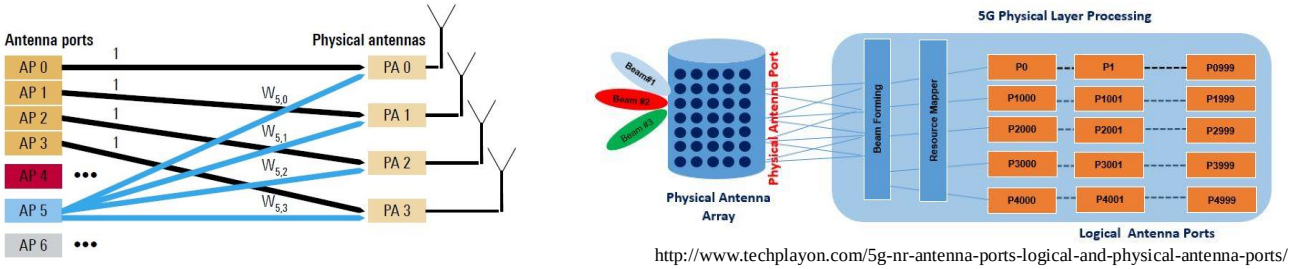

http://www.techplayon.com/5g-nr-antenna-ports-logical-and-physical-antenna-ports/

Fig. 4 – Mapping of Logical Antenna Ports to Physical Transmit Antennas in 4G LTE (Left, Rohde & Schwartz) and 5G NR (Right, Web)

Antenna Port (AP)

As shown in Fig. 3, each antenna port has a different arrangement of its CRS resource elements (REs). CRS appears in every slot: in the 1st and 5th OFDM symbols for antenna ports 0 and 1 and in the 2nd OFDM symbol for antenna ports 2 and 3. The density of CRS for the last two antenna ports (2 and 3) is half of that for the first two (0 and 1) to reduce the system overhead. The CRS antenna ports can be configured for 2- or 4-port transmit diversity and 2-, 3-, or 4-port spatial multiplexing. We mostly encounter antenna ports 0 and 1 in our experimental data presented in this paper.

Antenna ports do not correspond to physical antennas per se but rather they are logical entities distinguished by the reference signal sequences transmitted through them. From a receiver's perspective, two transmitted signals have experienced the same radio channel if and only if they are transmitted from the same antenna port [30]. In other words, each antenna port is associated with a specific reference signal and a receiver can thus use this reference signal to estimate the channel corresponding to the specific antenna port regardless of its physical origin.

In practice, an antenna port is implemented either as a single physical antenna (e.g. AP0, 1, 2, 3 in Fig. 4) or as a combination of multiple physical antenna elements (e.g. AP5 in Fig. 4) [31]. A receiver derives a channel estimate for all data transmitted on the same antenna port regardless of whether it represents a single radio channel from one physical antenna or a composite channel from a multiplicity of physical antenna elements together constituting the antenna port.

Clearly, the use of antenna ports does not cause any problem in channel estimation and subsequent data decoding for communications. However, it may present a potential ambiguity as to where the physical transmit antenna's phase center is for the purpose of precise ranging. From a user's point of view and for the purpose of timing/ranging, we investigate the effect of AP on TOA estimation and its practical implications.

Cell-Specific Reference Signal (CRS)

In LTE, the arrangement of the REs on which a CRS sequence is transmitted has the goal to achieve minimum mean squared error (MMSE) estimation of the channel under high mobility assumptions [30]. The spacing of reference elements in time is determined by the maximum Doppler spread (clock drift) the signal is expected to experience. For a speed of 500 km/h, the Doppler shift is $f_d \approx 950$ Hz at a center frequency of 2 GHz. The minimum Nyquist sampling rate is $T_s = 1/(2f_d) \approx 0.5$ ms, which is the duration of a timeslot. As such, antenna ports 0 and 1 have two reference elements per slot (at symbols 0 and 4) and antenna ports 2 and 3 have one reference element per slot (at symbol 1) in order to estimate the channel correctly.

As shown in Fig. 3, one reference element (RE) is placed every six subcarriers on each CRS OFDM symbol but the reference elements are staggered so that within a resource block (RB), a reference element is placed every three subcarriers. This spacing is related to the expected coherence bandwidth of the channel, which in turn is tied to the channel delay spread. The maximum root mean squared (RMS) channel delay spread considered for LTE is $\sigma_t = 991$ ns. The corresponding 90% and 50% coherent bandwidths are $B_{c,90\%} = 1/(50\sigma_t) = 20$ kHz and $B_{c,50\%} = 1/(5\sigma_t) = 200$ kHz, respectively, where $B_{c,x\%}$ is defined as the bandwidth at which the autocorrelation function of the channel in the frequency domain is equal to x% of the peak. The spacing between

two reference elements in frequency is 45 kHz (3 subcarriers) in one RB and 90 kHz (6 subcarriers) in an OFDM symbol, thus allowing the expected frequency-domain variations of the channel to be resolved.

According to [1], a reference-signal sequence $r_{l,n_s}(m)$ is defined by

$$r_{l,n_s}(m) = \frac{1}{\sqrt{2}}\big(1 - 2 \cdot c(2m)\big) + j\frac{1}{\sqrt{2}}(1 - 2 \cdot c(2m+1)),\ m = 0,1,\dots,2 \cdot N_{RB}^{max,DL} - 1 \quad (2)$$

where n_s = 0 to 19 is the slot number within a radio frame, l = 0, 1, or 4 is the OFDM symbol number within the slot, and $N_{RB}^{max,DL}$ = 110 is the maximum number of resource blocks for downlink. The pseudo-random sequence $c(n)$ is defined by a length-31 Gold sequence as

$$c(n) = \big(x_1(n+N_c) + x_2(n+N_c)\big) mod 2 \quad (3a)$$
$$x_1(n+31) = \big(x_1(n+3) + x_1(n)\big) mod 2 \quad (3b)$$
$$x_2(n+31) = \big(x_2(n+3) + x_2(n+2) + x_2(n+1) + x_2(n)\big) mod 2 \quad (3c)$$

where N_c = 1600, the first m-sequence is initialized with $x_1(0) = 1$ and $x_1(n) = 0$ for n = 1, 2, …, 30, and the second m-sequence is initialized at the start of each OFDM symbol by

$$c_{init} = \sum_{i=0}^{30} x_2(i) \cdot 2^i = 2^{10} \cdot (7 \cdot (n_s' + 1) + l + 1) \cdot \big(2 \cdot N_{ID}^{cell} + 1\big) + 2 \cdot N_{ID}^{cell} + N_{CP} \quad (3d)$$

$$n_s' = \begin{cases} 10\lfloor n_s/10 \rfloor mod 2, & \text{for frame structure type 3 when CRS is part of a DRS} \\ n_s, & \text{otherwise} \end{cases} \quad (3e)$$

$$N_{CP} = \begin{cases} 1, & \text{for normal CP} \\ 0, & \text{for extended CP} \end{cases} \quad (3f)$$

Note that frame structure type 1/2/3 is used for FDD/TDD/licensed assisted access (LAA), respectively. The reference-signal sequence $r_{l,n_s}(m)$ is then mapped to complex-valued modulation symbols $a_{k,l}^{(p)}$ used as reference symbols for antenna port p in slot n_s according to

$$a_{k,l}^{(p)} = r_{l,n_s}(m') \quad (4a)$$

where

$$k = 6m + \big(v + v_{shift}\big) mod 6 \quad (4b)$$

$$l = \begin{cases} 0, N_{symb}^{DL} - 3, & \text{if } p \in [0,1] \\ 1, & \text{if } p \in [2,3] \end{cases},\ N_{symb}^{DL} = 7 \text{ for } N_{CP} = 1 \text{ (normal CP)} \quad (4c)$$

$$m = 0,1,\dots,2 \cdot N_{RB}^{DL} - 1 \quad (4d)$$

$$m = m' + N_{RB}^{max,DL} \cdot N_{RB}^{DL} \quad (4e)$$

The variables v and v_{shift} define the position in the frequency domain for the different reference signals with v given by

$$v = \begin{cases} 0 & \text{if } p = 0 \text{ and } l = 0 \\ 3 & \text{if } p = 0 \text{ and } l \neq 0 \\ 3 & \text{if } p = 1 \text{ and } l = 0 \\ 0 & \text{if } p = 1 \text{ and } l \neq 0 \\ 3(n_s mod 2) & \text{if } p = 2 \\ 3 + 3(n_s mod 2) & \text{if } p = 3 \end{cases} \quad (5a)$$

And the cell-specific frequency shift given by

$$v_{shift} = N_{ID}^{cell} mod 6 \quad (5b)$$

Clearly, the generation of a CRS sequence depends on (i) PCI N_{Id}^{Cell}, (ii) the slot number in a frame (n_s = 0 to 19), (iii) the OFDM symbol number in a slot (l = 0, 1, or 4), and (iv) the antenna port (p = 0, 1, 2, 3). A different CRS sequence is therefore designed for a different antenna port to minimize the intra-cell interference between multiple transmit antenna ports. When an RE is used to transmit a CRS on an antenna port, the corresponding RE on the other antenna ports is set to zero. Also note that a cell-specific frequency shift is applied to the CRS patterns to help avoid time-frequency collisions of CRS from up to six adjacent cells. The transmission of CRS may be boosted in power by 6 dB relative to surrounding data symbols.

An example of a CRS OFDM symbol is shown in Fig. 5. It is specified in the frequency domain as shown in Fig. 5(a) for N_{Id}^{Cell} = 17, n_s = 19, l = 0, p = 0 with N_{rb} = 6 (the basic six RBs within 1.4 MHz). CRS sequences are QPSK-modulated and Fig. 5(b) shows the complex CRS waveform in the time domain where six clusters are visible. But its magnitude is not constant with a visible periodicity as shown in Fig. 5(c).

The autocorrelation function of a CRS OFDM symbol (N_{Id}^{Cell} = 0, n_s = 0, l = 0, p = 0, N_{rb} = 6) is shown in Fig. 5(d). Since the CRS sequences are inserted once every 6 subcarriers for a CRS OFDM symbol in the frequency domain, their time-domain waveform has a periodicity of $N_u/6$ as shown in Fig. 5(b) so is their correlation function having six peaks in Fig. 5(d). As long as the initial timing error is less than one twelfth of an OFDM symbol duration ($\pm T_u/12$), there is no ambiguity in determining the correlation peak.

When the subcarriers in two consecutive CRS OFDM symbols are coherently summed, the resulting correlation function has a periodicity of $N_u/3$ as shown in Fig. 5(e), due to the fact that the aggregated spectrum has a spacing of 3 subcarriers. The correlation peak maintains the same shape but the peak is doubled and the ambiguity interval is doubled as well.

Fig. 5(f) shows the details of the correlation peaks for different numbers of resource blocks N_{rb} = 6, 15, 25, 50, 75, and 100, respectively, as listed in Table 1. For a larger N_{rb}, its correlation peak is narrower because of a wider system bandwidth.

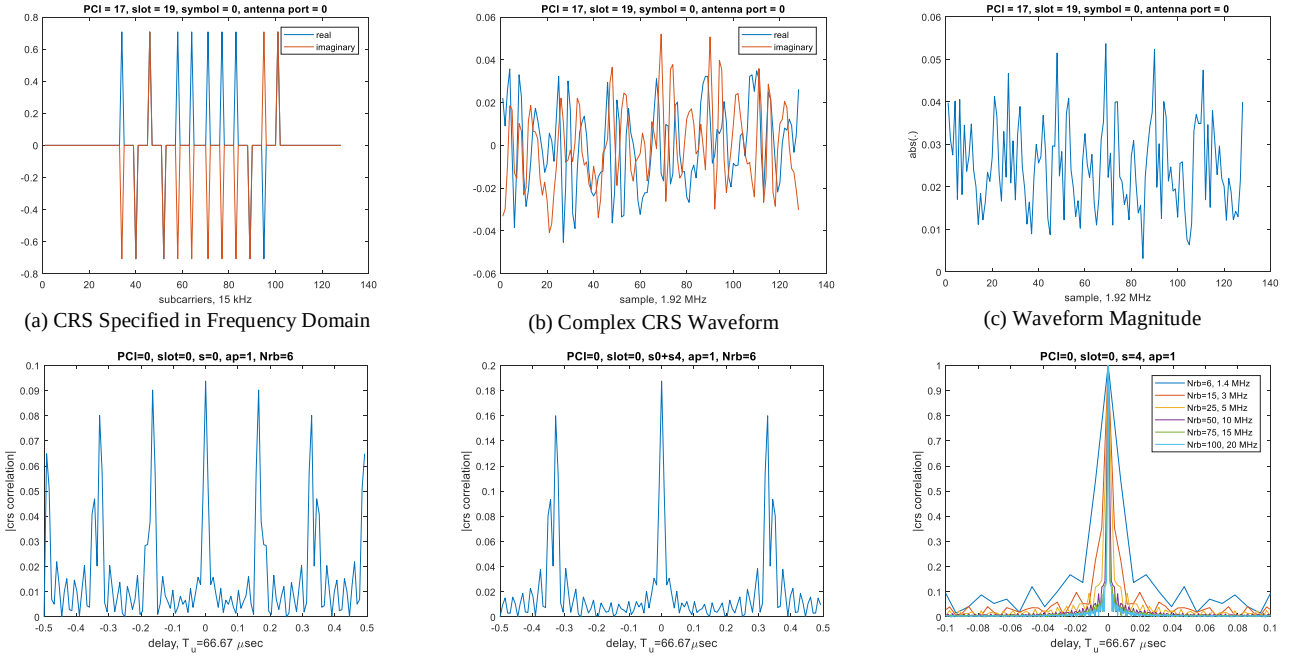

(a) CRS Specified in Frequency Domain (b) Complex CRS Waveform (c) Waveform Magnitude

(d) CRS Correlation Function for Symbol 0 (e) Correlation Function for Symbols 0 and 4 (f) Correlation Peaks for Different Bandwidths

Fig. 5 – Ideal Correlation Functions of CRS OFDM Symbol

Channel Impulse Response (CIR)

To extract an OFDM symbol that contains CRS from the incoming signal, one needs to first obtain the frame timing, slot boundary, and symbol boundary for a given PCI and an antenna port as described in the previous section. The FFO estimated from CP or PSS/SSS can be applied to the signal samples prior to CRS correlation. The integer frequency offset (IFO), if having not been done yet, can be estimated and removed during the CRS correlation process either in the time domain or frequency domain.

Denote a time-domain CRS sequence by $crs_{n_s,l}^{(i,p)}(n)$ where i is the cell ID N_{Id}^{Cell}, p is the antenna port, n_s is the slot number, l is the OFDM symbol number within a slot, and n is the signal sample index of the OFDM symbol for CRS; and $CRS_{n_s,l}^{(i,p)}(k) = FFT_n^k\{crs_{n_s,l}^{(i,p)}(n)\}$ is the CRS sequence in the frequency domain with k being the subcarrier index. Detection of CRS can be performed as a two-dimensional search with the FFT-implemented circular correlation, also referred to as channel impulse response (CIR), as

$$(\hat{\tau}, \hat{\varepsilon}_i) = arg \max_{\tau,\varepsilon_i} \left| cir_{n_s,l}^{(i,p)}(\tau, \varepsilon_i) \right|, \varepsilon_i \in \{0, \pm 1, \dots\} \quad (6a)$$

$$cir_{n_s,l}^{(i,p)}(\tau, \varepsilon_i) = IFFT_k^\tau\{FFT_n^k\{r_{n_s,l}^{(i,p)}(n)\} \cdot (CRS_{n_s,l}^{(i,p)}(k + \varepsilon_i))^*\} \quad (6b)$$

where $FFT_n^k\{r_{n_s,l}^{(i,p)}(n)\} \rightarrow R_{n_s,l}^{(i,p)}(k)$ is the FFT of the extracted CRS OFDM symbol samples and $IFFT_k^\tau\{.\}$ is the inverse fast Fourier transform (IFFT) from the input frequency index k to the output time index τ.

A refined FFO estimate can also be obtained from the phase difference symbols of the same subcarriers between two adjacent CRS in the frequency domain, averaged over a frame, as

$$\hat{\varepsilon}_f = \frac{N_u}{2\pi N_{slot}} \angle \frac{1}{N_{sc} N_{crs} N_{ap} (N_s - 1)} \sum_{n_s=0}^{N_s} \sum_{p=0}^{N_{ap}} \sum_{l=0}^{N_{crs}} \sum_{k=0}^{N_{sc}} \left(R_{n_s+1,l}^{(i,p)}(k) \left(CRS_{n_s+1,l}^{(i,p)}(k) \right)^* \right) \left(R_{n_s,l}^{(i,p)}(k) \left(crs_{n_s,l}^{(i,p)}(k) \right)^* \right)^* \quad (7)$$

where N_{sc} is the number of phase differences integrated in the innermost summation after excluding null subcarriers (DC ad guard subcarriers), N_u is the number of useful samples in an OFDM symbol, N_{slot} is the number of samples per slot, N_{crs} is the number of CRS symbols used in the integration, N_{ap} is the number of antenna ports used in the integration, and N_s is the number of slots per frame.

In a slot, there are up to six CRS sequences that can be used to generate six CIRs: two on OFDM symbol 0 for antenna ports 0 and 1, two on OFDM symbol 1 for antenna ports 2 and 3, and two on OFDM symbol 4 for antenna ports 0 and 1 again. In our limited collection of data, we mostly encountered antenna ports 0 and 1 on symbols 0 and 4 and rarely antenna ports 2 and 3 on symbols 1. Note that CIR detection can be used to determine the slot number and symbol number via a multi-dimensional search if they have not already been determined from PSS and SSS yet or when an additional confirmation is required. One advantage of using CRS is that the signal is transmitted over the entire downlink bandwidth up to 20 MHz, not merely the basic bandwidth of 1.4 MHz available to PSS/SSS. Since our USRP is set to operate at f_s = 20 MHz, the possible bandwidths are 3, 5, and 10 MHz, the number of RBs N_{rb} = 15, 25, and 50, and the resampling rate f_s = 3.84, 7.68, and 15.36 MHz, respectively, in addition to the minimum bandwidth of 1.4 MHz, N_{rb} = 6, and the basic rate of 1.92 MHz as shown in Table 1.

Fig. 6 shows the effect of the downlink bandwidth (1.4, 3, 5, and 10 MHz) on CRS correlation on symbol 4 (Figs. 6(a), 6(b), 6(c), and 6(d)), respectively (similar results are observed for symbol 0, which are omitted here for simplicity). With a wider bandwidth, the correlation peak is sharper and the SNR is higher, consistent with the observation of Fig. 5(f). Furthermore, a sharper peak reveals more details related to motion and/or multipath (e.g., the double peaks in Fig. 6(d)).

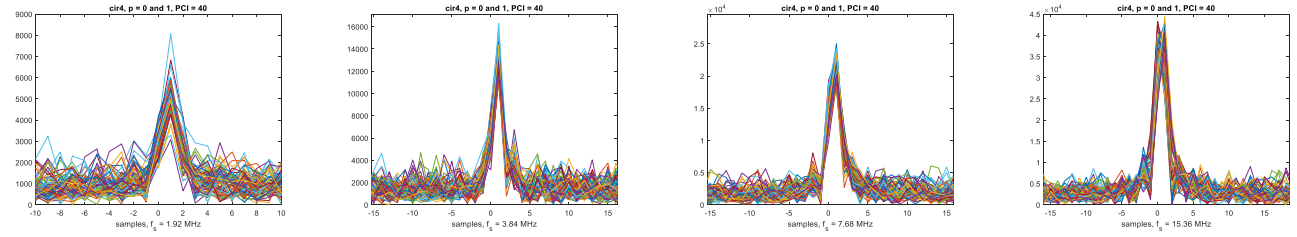

(a) Symbol 4, AP 0 and 1, N_{rb} = 6 (b) Symbol 4, AP 0 and 1, N_{rb} = 15 (c) Symbol 4, AP 0 and 1, N_{rb} = 25 (d) Symbol 4, AP 0 and 1, N_{rb} = 50

Fig. 6 – Correlation Functions of CRS on OFDM Symbols 0 and 4 for Antenna Ports 0 and 1 under Different Downlink Bandwidths

For the case shown in Fig. 7(a), CRS is searched at OFDM symbols 0, 1, and 4 for antenna ports 0, 1, 2, 3 but only the CIR for antenna port 0 CIR is detected at symbols 0 and 4. It was found that when two cells are detected, their frames are off by one slot in frame timing. As such, their CRS OFDM symbols coincide in time but do not overlap in frequency due to frequency-domain orthogonality. Furthermore, in Figs. 7(b) and 7(c), the CIR over 62 slots (more than 30 ms) are shown for symbols 0 and 4 at antenna ports 0 and 1 for PCI = 307. Similarly, in Figs. 7(d) and 7(e), the CIR over 62 slots (more than 30 ms) are shown for symbols 0 and 4 at antenna ports 0 and 1 for PCI = 39, where a secondary peak due to multipath is visible.

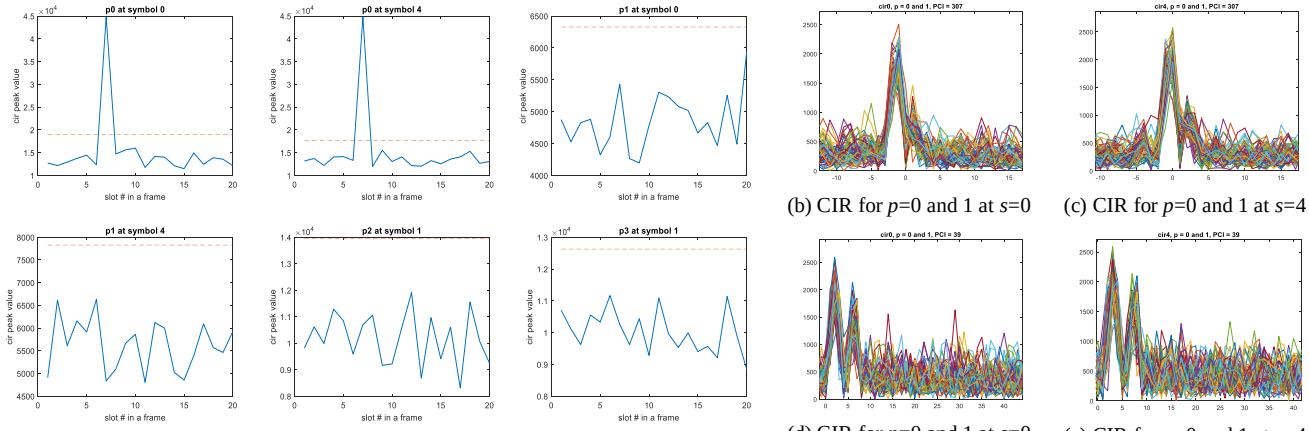

(a) CRS is searched at OFDM symbols 0, 1, and 4 for antenna ports 0, 1, 2, 3 (b) CIR for p=0 and 1 at s=0 (c) CIR for p=0 and 1 at s=4 (d) CIR for p=0 and 1 at s=0 (e) CIR for p=0 and 1 at s=4

Fig. 7 – Correlation Functions of CRS on OFDM Symbols 0 and 4 for Antenna Ports 0 and 1 Subject to Multipath

The peak location of LTE CRS correlation can be tracked with a delay lock loop (DLL) [20] similar to that of DVB pilot subcarriers [13]. Similarly, the FFO estimate in (7) can be used to initialize a frequency lock loops (FLL) to track the LTE

signal [33] in a manner similar to DVB signals [34, 35]. The complex CRS correlation, when viewed as a prompt correlator, can be used to drive a phase error discriminator to a phase lock loop (PLL) [25, 36].

EFFECT OF AP ON TOA ESTIMATION IN MULTIPATH AND DIVERSITY

In this section, the effect of antenna ports on TOA estimation for pseudorange generation in the presence of multipath and NLOS signals is discussed.

TOA Estimation with Multipath and NLOS Signals for Different Antenna Ports

Four TOA estimates from four CRS sequences on symbols 0 and 4 for antenna ports 0 and 1 are shown in Fig. 8 with typical error patterns for "peak-picking." Fig. 8(a) shows the TOA measured from the correlation functions shown in Fig. 8(e) at slot 1539 for the 4 CRS sequences, the four TOA estimates are only off by a fractional of a sample at the resampling rate of 15.36 MHz corresponding to the system bandwidth of 10 MHz with N_{rb} = 50 as shown in Table 1.

Fig. 8(b) shows the TOAs at slot 112558, which show an outlier for antenna port 1 at symbol 0. As shown in Fig. 8(f), for this slot, the signals on antenna port 1 are lower than those on antenna port 0. In particular, a multipath component exceeds the threshold while the direct signal is lower than the threshold as shown in the second subplot of Fig. 7(f).

At slot 292718, only the peak for antenna port 1 at symbol 4 barely passes the threshold as shown in Fig. 8(g), while the other three are faded. Peak-picking is meaningless, leading to large outliers as shown in Fig. 8(c).

It is interesting to note that the correlation functions for antenna port 0 are similar at symbols 0 and 4 (stability in time) so are those for antenna port 1 as shown in Fig. 8(h), which is consistent with the definition of antenna ports. However, for antenna port 0, the first peaks (likely the direct signal) dominate while for antenna port 1, the second peaks (a multipath signal) dominate. Peak-picking leads to different TOA estimates as shown in Fig. 8(d). This is an example showing the effect of antenna ports on TOA estimation in the presence of multipath.

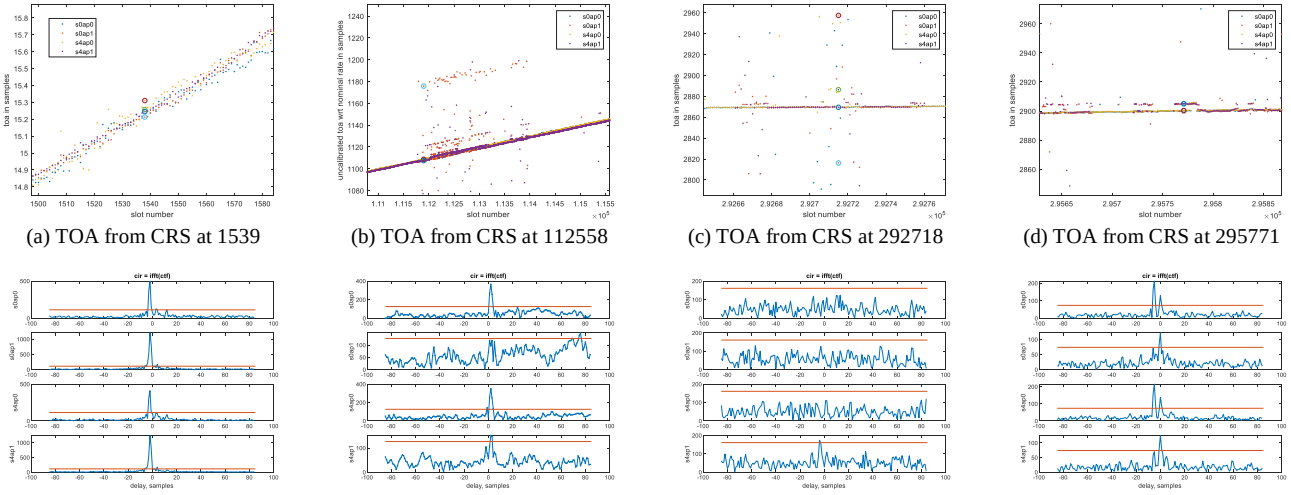

(a) TOA from CRS at 1539 (b) TOA from CRS at 112558 (c) TOA from CRS at 292718 (d) TOA from CRS at 295771

(e) CRS Correlations at 1539 (f) CRS Correlation at 112558 (g) CRS Correlation at 292718 (h) CRS Correlation at 295771

Fig. 8 – TOA Errors for Different Antenna Ports When "Peak-Picking" of CRS Correlations Prone to Outliers Due to Fading and NLOS

Alternative to "peak-picking" is the "first arrival" method for TOA estimation. Fig. 9 shows several examples, which illustrate the variability in TOA estimation. In Case A, the first peaks (purple circle) coincide with the max peaks (yellow cross) for antenna port 1 on symbols 0 and 4, short-handed as S0AP1 and S4AP1, in Figs. 9(e) and 8(m), respectively. However, for antenna port 0 on symbols 0 and 4, short-handed as S0AP0 and S4AP0, in Figs. 9(a) and 9(i), respectively, the max peaks differ from the first peaks and there are also additional peaks due to multipath. In this case, the first arrival method provides consistent TOA estimates across the 4 CRS sequences. Also note for this case that the transmission channel characterized by antenna port 1 is cleaner than that of antenna port 0.

In Case B, the first arrival peaks are detected for S0AP1 and S4AP1 in Figs. 9(f) and 9(n). However, the apparent arrival peaks for S0AP0 and S4AP0 are below the threshold as shown in Figs. 9(b) and 9(j) even though they are visible. Lowering the detection threshold runs the risk of an increased false alarm rate as shown in Fig. 9(c) for Case C. Is it a first arrival detection or a false detection?

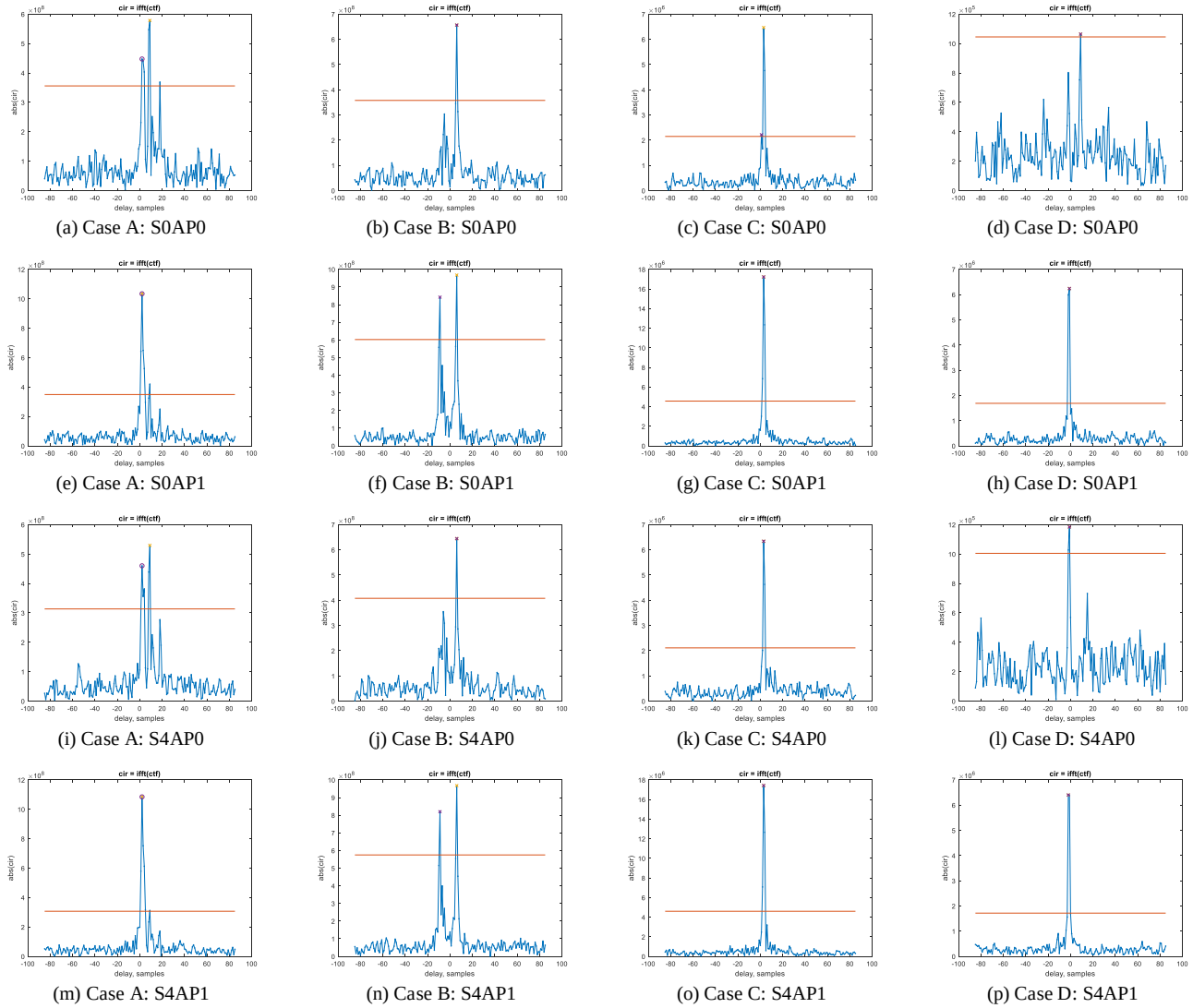

(a) Case A: S0AP0 (b) Case B: S0AP0 (c) Case C: S0AP0 (d) Case D: S0AP0

(e) Case A: S0AP1 (f) Case B: S0AP1 (g) Case C: S0AP1 (h) Case D: S0AP1

(i) Case A: S4AP0 (j) Case B: S4AP0 (k) Case C: S4AP0 (l) Case D: S4AP0

(m) Case A: S4AP1 (n) Case B: S4AP1 (o) Case C: S4AP1 (p) Case D: S4AP1

Fig. 9 – "Peak-Picking" vs. "First Arrival" for TOA Determination for Different Antenna Ports in Multipath Environments

Case D is another example where antenna port 0 is noisier than antenna port 1. The S4AP0 peak in Fig. 9(l) is definite. However, the max peak of S0AP0 in Fig. 9(d) seems to be multipath while the first arrival is only slightly above other spurious peaks.

From the examples in Figs. 8 and 9, it is clear that due to mobile fading, the direct signal does not always appear on all CRS OFDM symbols for all antenna ports, and a verification (signal detection) is therefore necessary before measuring peak TOA.

The CRS correlation peak location can be used to initialize a DLL to track the delay of the dominant signal for refined TOA estimation. However, a more elaborate method to estimate the parameters of multiple peaks in correlation (multipath and NLOS components) is to apply the matching pursuit (MP) algorithm [37] to the channel impulse response [13, 14] in the time domain or the order-recursive least-square matching pursuit algorithm [38, 39, 40] and MUSIC/ESPRIT methods [25] to the channel transfer function [21] in the frequency domain [27]. Similar methods were used earlier for GNSS signals [41, 42, 43].

AP Effect on Pseudorange Measurements

The TOA estimates shown above are the raw measurements obtained in an open loop manner via peak-picking of the CRS correlation per OFDM symbol per antenna port without any filtering. These TOA estimates are at a rate of 2000 Hz (0.5 ms per slot) and can be viewed as the output of a code delay error discriminator.

Fig. 10(a) shows the four pseudoranges for PCI = 349 at 2135.2 MHz (antenna ports 0 and 1 on symbols 0 and 4) after removing the clock bias and drift, which are estimated based on stationary data in the first 30 seconds. There are slight differences (fractional samples) between symbols 0 and 4 for the same antenna port but large differences (2 ~ 3 samples, 19.52 m/sample

at 15.36 MHz) between different antenna ports. Details for four data segments are shown in Figs. 10(b), 10(c), 10(d), and 10(e), respectively. It seems that the measurements from antenna port 1 are more stable than from antenna port 0. There are sporadic large outliers, frequent small multipath offsets, persistent NLOS structures, and data gaps due to fading. Outliers are legitimate detections for the chosen detection threshold. The clear and stable NLOS structures may be used for multipath exploration [44].

Fig. 11(a) show the four calibrated pseudoranges for PCI = 39 at 2135.2 MHz and details of four data segments are shown in Figs. 11(b), 11(c), 11(d), and 11(e), respectively. The observations made for Fig. 10 hold for Fig. 11, namely, there are slight differences (fractional samples) between symbols 0 and 4 for the same antenna port but large differences (2 ~ 3 samples) between different antenna ports. It is another example showing the effect of antenna ports on pseudorange measurements derived from TOA estimation using CRS sequences on symbols 0 and 4 per slot in the presence of multipath.

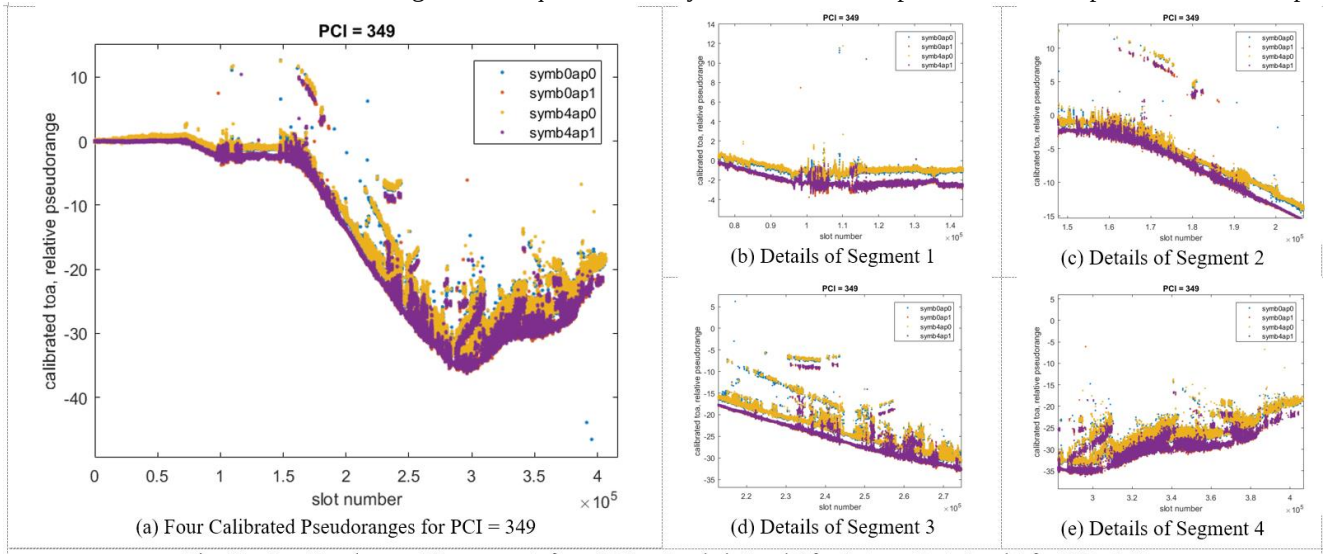

(a) Four Calibrated Pseudoranges for PCI = 349

(b) Details of Segment 1

(c) Details of Segment 2

(d) Details of Segment 3

(e) Details of Segment 4

Fig. 10 – Raw Pseudorange Measurements from CRS on Symbols 0 and 4 for Antenna Ports 0 and 1 for PCI = 349

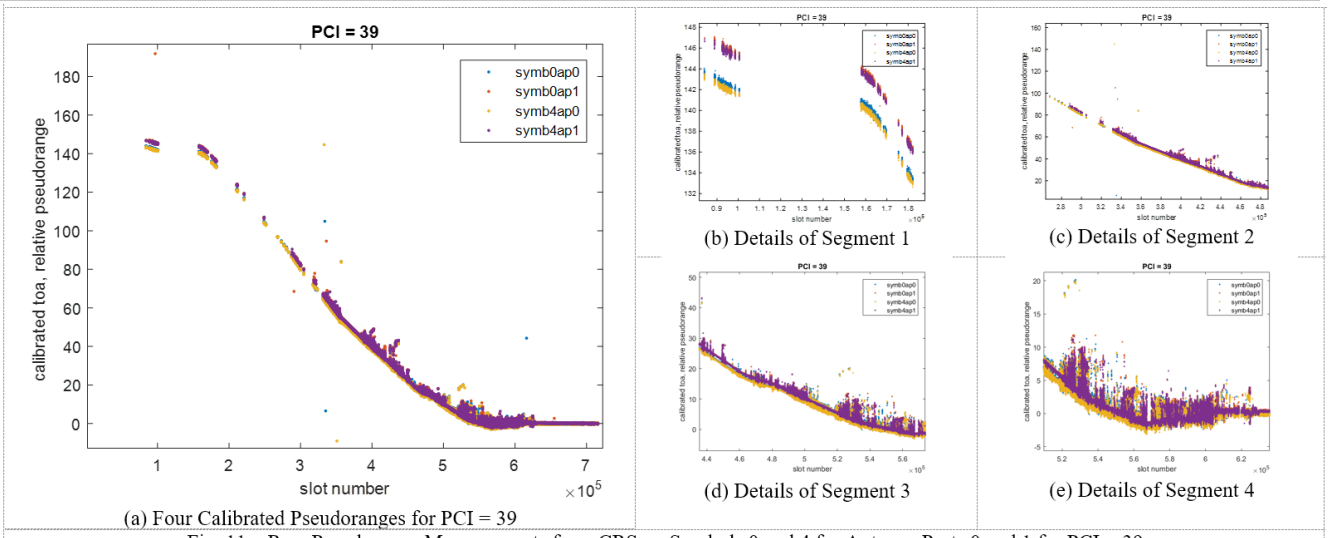

(a) Four Calibrated Pseudoranges for PCI = 39

(b) Details of Segment 1

(c) Details of Segment 2

(d) Details of Segment 3

(e) Details of Segment 4

Fig. 11 – Raw Pseudorange Measurements from CRS on Symbols 0 and 4 for Antenna Ports 0 and 1 for PCI = 39

Low-pass filtering can be applied to raw pseudorange measurements so as to reject outliers (gating) and smooth out high-frequency jitters (averaging). Fig. 12(a) show the four pseudoranges for PCI = 349 at 2135.2 MHz (antenna ports 0 and 1 on symbols 0 and 4) filtered with a two-state constant velocity Kalman filter (a second order low-pass filtering). Again, there are slight differences (fractional samples) between symbols 0 and 4 for the same antenna ports but rather large differences (2 ~ 3 samples, 19.52 m/sample at 15.32 MHz) between different antenna ports.

Raw and filtered pseudoranges are compared for antenna port 0 on symbol 0 and antenna port 1 on symbol 4 with details for four data segments shown in Figs. 12(b), 12(c), 12(d) and 12(e)), respectively. It can be seen that even though the filter is able

to fill the data gaps, reject outliers, and smooth out the noise, the estimate may jump to multipath components and be carried away by the presence of persistent NLOS signals, leading to large ranging errors.

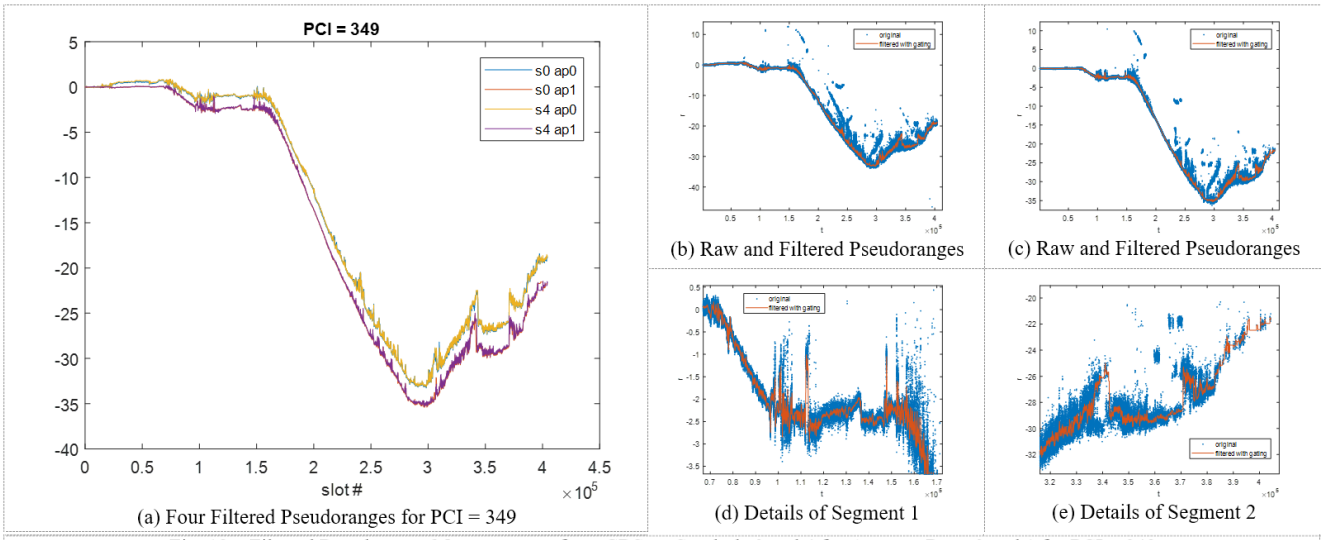

(a) Four Filtered Pseudoranges for PCI = 349 (b) Raw and Filtered Pseudoranges (c) Raw and Filtered Pseudoranges (d) Details of Segment 1 (e) Details of Segment 2

Fig. 12 – Filtered Pseudorange Measurements from CRS on Symbols 0 and 4 for Antenna Ports 0 and 1 for PCI = 349

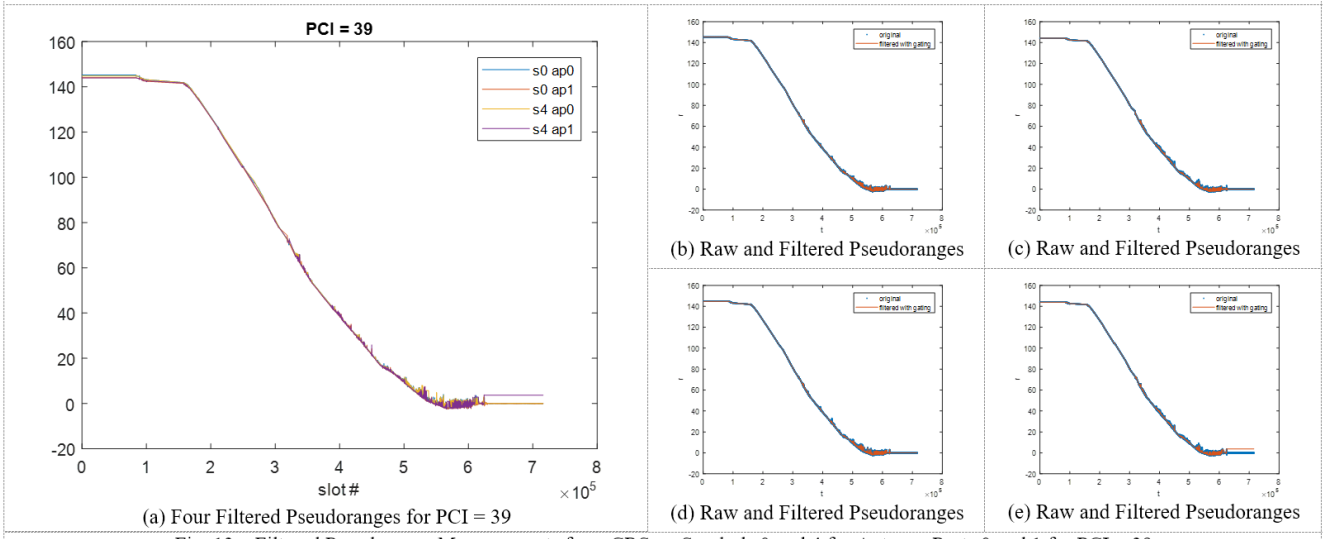

(a) Four Filtered Pseudoranges for PCI = 39 (b) Raw and Filtered Pseudoranges (c) Raw and Filtered Pseudoranges (d) Raw and Filtered Pseudoranges (e) Raw and Filtered Pseudoranges

Fig. 13 – Filtered Pseudorange Measurements from CRS on Symbols 0 and 4 for Antenna Ports 0 and 1 for PCI = 39

Fig. 13(a) show the four filtered pseudoranges for PCI = 39. Raw and filtered pseudoranges are compared for antenna ports 0 and 1 on symbols 0 and 4 in Figs. 13(b), 13(c), 13(d), and 13(e), respectively. Observations made for Fig. 12 regarding the effects of multipath and NLOS signals for different antenna ports are valid for Fig. 13 as well.

With pseudoranges to two cell towers as shown in Fig. 1, though not ideal, it is possible to obtain initial position fixes along the test trajectory provided that a known static position cell tower clock calibration is carried out. The mobile positioning results will be presented in [46].

The experimental data clearly show the effect of antenna ports. It leads to different behaviors of correlation functions using CRS sequences for different antenna ports in the presence of multipath and to large differences in TOA estimates/pseudorange measurements with CRS between antenna ports. In our low dynamic tests, the temporal difference between symbols 0 and 1 is not obvious. Such conditional stationarity may be used to coherently combine symbols 0 and 1 if carrier phase variations can be accounted for. However, the difference is quite large in frequency and space. Such differences are the desired result of diversity sought for by the design of antenna ports in the first place: temporal in different symbols, spectral in different subcarriers, and spatial in different combinations of physical antennas. The channel is thus sufficiently sampled (at the Nyquist

rate) and the best one or their combination is used for data transmission. The exploitation of such diversity and its benefits is a new frontier for ranging and positioning.

CONCLUSIONS

In this paper, we analyzed 4G LTE experimental data and investigated the effect of antenna ports on TOA estimation using CRS sequences. Fading occurred frequently in our mobile testing suburban environment where multipath signals were abundant and NLOS structures were rather stable. Pseudoranges were derived from TOA estimates after removing clock bias and drift based on an initial static data calibration. As shown in our data, the channel responses were different for different antenna ports. Thought not being an issue for channel estimation and data decoding for communications, it may present a potential ambiguity as to where the physical transmit antenna's phase center is for precision ranging.

The availability of multiple TOA estimates/pseudorange measurements obtained from CRS sequences associated with different antenna ports is not merely redundancy but also diversity for ranging and positioning. Surely it brings more complexity in processing. The phase center for each antenna port, be it a physical antenna or a combination of many antennas, needs to be determined especially for carrier phase-based precision ranging. The offset in TOA/pseudoranges between different antenna ports needs to be estimated (calibrated off) if one wants to use all measurements in positioning. Nevertheless, it offers the opportunity of diversity processing, not known previously, to obtain the best measurements for positioning in the presence of multipath and NLOS outliers.

The 4G LTE processing system presented in this paper will be integrated into the University GNSS software receiver MuSNAT [45] to allow combined GNSS/LTE signal processing and positioning. The used USRP frontend supports combined LTE+GNSS signal band reception. The MuSNAT signal processing algorithms are tailored for GNSS signal processing but can be adapted for LTE signals. Another direction of future work is to extend the signal processing framework described in this paper to 5G NR signals.

ACKNOWLEDGEMENTS

We would like to acknowledge the support of the Bundesnetzagentur in supporting this activity. Part of this work was carried out within the DLR funded project "Galileo FUSION". Thanks also go to Stephan Ullrich for his efforts in collecting all the experimental data.

REFERENCES

[1] 3GPP TS 36.211 – v14.2.0, *Physical Channels and Modulation*, (Release 14), April 2017.

[2] L. Korowajczuk, *LTE, WiMAX and WLAN Network Design, Optimization and Performance Analysis*, John Wiley & Sons, Ltd, 2011.

[3] J.B. Kenney, "Dedicated Short-Range Communications (DSRC) Standards in the United States," *Proceedings of the IEEE*, Vol. 99, No. 7, July 2011, 1162-1182.

[4] ETSI EN 300 744 V1.5.1, *Digital Video Broadcasting (DVB); Framing Structure, Channel Coding and Modulation for Digital Terrestrial Television* (2004-06).

[5] ARIB STD-B31 Version 1.6, *Transmission System for Digital Terrestrial Television Broadcasting*, November 30, 2005

[6] GB 20600—2006, *Framing Structure, Channel Coding and Modulation for Digital Television Terrestrial Broadcasting System*, Effective 2007-08-01, Published 2006-08-18.

[7] ATSC Standard, *System Discovery and Signaling*, Doc. A/321:2016, 23 March 2016.

[8] D. Garmatyuk and K. Kauffman, "Radar and Data Communication Fusion with UWB-OFDM Software-Defined System," *Proc. of IEEE International Conference on Ultra-Wideband*, Sept. 2009.

[9] M. Rabinowitz and J.J. Spilker, Jr., "A New Positioning System Using Television Synchronization Signals*," IEEE Trans. on Broadcasting*, 51(1), 51–61, March 2005.

[10] M. Martone and J. Matzler, "Prime Time Positioning Using Broadcast TV Signals to Fill in GPS Acquisition Gap," *GPS World*, Sept. 2005, 52-60.

[11] X. Ji, Y. Zhang, J. Wang, L. Dai, "Time-Frequency Joint Positioning for Chinese Digital Television Terrestrial Broadcasting System," *12th IEEE Int. Conf. on Communication Technology*, Nanjing, Nov. 2010, 950-953.

[12] W. Li, H. Wu, D. Ucci, and Y. Morton, "A Positioning System Using Chinese Digital TV Signals under Limited GPS Signal Observability Conditions in Urban Environment," *ION 2010 Int. Technical Meeting*, January 2010, San Diego, CA, 264-269.

[13] D. Serant, O. Julien, L. Ries, P. Thevenon, and M. Dervin, "The Digital TV Case – Positioning with Signals of Opportunity Based on OFDM Modulation," *InsideGNSS*, Nov/Dec 2011, 54-62.

[14] P. Thevenon, S. Damien, O. Julien, C. Macabiau, M. Bousquet, L. Ries, Lionel, and S. Corazza, "Positioning Using Mobile TV Based on the DVB-SH Standard," *Navigation: Journal of the Institute of Navigation*, Vol. 58, No. 2, Summer 2011, 71-90.

[15] L. Dai, Z. Wang, C. Pan, and S. Chen, "Wireless Positioning Using TDS-OFDM Signals in Single Frequency Networks," *IEEE Trans. on Broadcasting*, Vol. 58. No. 2, June 2012, pp 236-246.
[16] J. Huang and L.L. Presti, "DVB-T Positioning with a One-Shot Receiver," *2013 Int. Conf. on Localization and GNSS*, Turin, pp 1-5.
[17] C. Yang, T Nguyen, and E. Blasch, "Mobile Positioning via Fusion of Mixed Signals of Opportunity," *IEEE AES Magazine*, 2014.
[18] P. Gadka, "New First Path Detector for LTE Positioning Reference Signals," UBICOMM 2014, *the 8th Int. Conf. on Mobile Ubiquitous Computing, Systems, Services and Techniques*, 2014.
[19] C. Yang and T. Nguyen, "Tracking and Relative Positioning with Mixed Signals of Opportunity," *Navigation: Journal of the Institute of Navigation*, Vol. 62, No. 4, 291-311, Winter 2015.
[20] F. Knutti, M. Sabathy, M. Driusso, H. Mathis, and C. Marshall, "Positioning Using LTE Signals," *European Navigation Conference*, Bordeaux, France, April 2015.
[21] L. Chen, O. Julien, P. Thevenon, D. Serrant, A.G. Pena, and H. Kuusniemi, "TOA Estimation for Positioning with DVB-T Signals in Outdoor Static Tests," *IEEE Trans. on Broadcasting*, Vol. 61, No. 4, Dec. 2015, pp 625-638.
[22] M. Ulmschneider and C. Gentner, "Multipath Assisted Positioning for Pedestrians using LTE Signals," *Proc. of 2016 IEEE/ION Position, Location and Navigation Symposium - PLANS 2016*, April 2016.
[23] M. Driusso, C. Marshall, M. Sabathy, F. Knutti, H. Mathis, and F. Babich, "Vehicular Position Tracking Using LTE Signals," *IEEE Trans. on Vehicular Technology*, 66(4), 3376-3391, April 2017.
[24] C. Yang, L. Chen, O. Julien, and A. Soloviev, "Carrier Phase Tracking of OFDM-Based DVB-T Signals for Precision Ranging," *ION-GNSS+ 2017*, Portland, OR, September 2017.
[25] K. Shamaei and Z.M. Kassas, "LTE Receiver Design and Multipath Analysis for Navigation in Urban Environments," *Navigation: Journal of The Institute of Navigation*, Vol. 65, No. 4, Winter 2018, pp. 655-675.
[26] K. Shamaei, J. Khalife, and Z.M. Kassas, "Exploiting LTE Signals for Navigation: Theory to Implementation," *IEEE Trans. on Wireless Communications*, Vol. 17, No. 4, April 2018, pp. 2173-2189.
[27] C. Yang and A. Soloviev, "Positioning with Mixed Signals of Opportunity Subject to Multipath and Clock Errors in Urban Mobile Fading Environment," *ION GNSS+*, Sept 2018.
[28] T.D. Chiueh and P.Y. Tsai, *OFDM Baseband Receiver Design for Wireless Communications*, John Wiley & Sons, 2007.
[29] A. Zaidi, P. Athley, J. Medbo, U. Gustavsson, G. Durisi, and X. Chen, *5G Physical Layer Principles, Models and Technology Components*, Academic Press, Elsevier, 2018.
[30] E. Dahlman, S. Parkvall, and J. Skold, "Chapter 5: Physical Transmission Resources," in *4G, LTE-Advanced Pro and the Road to 5G* (3rd Ed.), Academic Press, Elsevier, 2016.
[31] A. Ancora, S. Sesia, and A. Gorokhov, "Chapter 8: Reference Signals and Channel Estimation," in *LTE – The UMTS Long Term Evolution: From Theory to Practice* (2nd Ed.), S. Sesia, I. Toufik, and M. Baker (Eds.), John Wiley & Sons, Ltd., 2011.
[32] K. Shi, E. Serpedin, and P. Ciblat, "Decision-Directed Fine Synchronization in OFDM Systems," *IEEE Trans. on Communications*, Vol. 53, No. 3, March 2005, 408-412.
[33] J.A. del Peral_rosado, J.A. Lopez-Salcedo, G. Seco-Granados, P. Crosta, F. Zanier, and M. Crisci, "Downlink Synchronization of LTE Base Stations for Opportunistic ToA Positioning," *2015 Int. Conf. on Localization and GNSS* (ICL-GNSS), June 2015.
[34] M. Speth, S. Fechtel, G. Fock, and H. Meyr, "Optimum Receiver Design for Wireless Broad-Band Systems Ysing OFDM – Part," *IEEE Trans. on Commu*nications, 47(11), April 1999.
[35] M. Speth, S. Fechtel, G. Fock, and H. Meyr, "Optimum Receiver Design for OFDM-Based Broadband Transmission – Part II: A Case Study," *IEEE Trans. on Communications*, 49(4), April 2001.
[36] J.A. del Peral-Rosado, J.A. Lopez-Salcedo and G. Seco-Granados, "Software-Defined Radio LTE Positioning Receiver Towards Future Hybrid localization Systems," *1st AIAA Int. Communications Satellite Systems Conf.*, Oct. 2013.
[37] S.F Cotter and B.D. Rao, "Spare Channel Estimation via Matching Pursuit with Application to Equalization," *IEEE Trans. on Communications*, Vol. 50, No. 3, 374-377, March 2002.
[38] W. Li and J.C. Preisig, "Estimation of Rapidly Time-Varying Sparse Channels," *IEEE J. of Oceanic Engineering*, Vol. 32, No. 4, 927-939, Oc. 2007.
[39] G.Z. Karabulut and A. Yongacoglu, "Sparse Channel Estimation Using Orthogonal Matching Pursuit Algorithm," *Proc. of IEEE VTC-Fall*, 3880-3884, 2014.
[40] I. Dockmanic and M. Vetterli, "OMP with Unknown Filters for Multipath Channel Estimation," *Signal Processing with Adaptive Sparse Structured Representations* (SPARS), No. EPFL-CONF-210571, 2015.
[41] C. Yang and M. Miller, "Novel GNSS Receiver Design Based on Satellite Signal Channel Transfer Function/Impulse Response," *Proc. of ION-GNSS'05*, Long Beach, CA, Sept. 2005.

[42] C. Yang, M. Miller, and T. Nguyen, "Symmetric Phase-Only Matched Filter (SPOMF) for Frequency-Domain Software GPS Receivers," *ION Journal: Navigation*, Vol. 54, No. 1, Spring 2007, pp 31-42 (ION Samuel M. Burka Award).
[43] C. Yang, T. Nguyen, and M. Miller, "GNSS Signal Channel Impulse Response Estimation: Modified Inverse Filter vs. Wiener Filter," *ION-GNSS'2009*, Savannah, GA, Sept. 2009.
[44] C. Gentner, T. Jost, and A. Dammann, "Accurate Indoor Positioning Using Multipath Components," *Proc. of ION GNSS+2013*, Nashville, TN, Sept. 2013.
[45] T. Pany, D. Dötterböck, H. Gomez-Martinez, M. Hammed, M. Subhan, F. Hörkner, T. Kraus, D. Maier, D. Sanchez-Morales, A. Schütz, P. Klima, D. Ebert, "The Multi-Sensor Navigation Analysis Tool (MuSNAT) – Architecture, LiDAR, GPU/CPU GNSS Signal Processing," *Proc. ION-GNSS+*, Miami, Florida, Sept. 2019, pp. 4087-4115.
[46] C. Yang, T. Pany, and P. Weitkemper, "Experimental Study of Cyclic and Reference Patterns in LTE Signals for TOA Estimation," Submitted to *ION-ITM*, San Diego, CA, January 2021.
[47] 3GPP TS38.211 5G New Radio — Physical Channels and Modulation, Version 15.2.0 Release 15, July 2018.